Cocktail of reactive species generated by cold atmospheric plasma : oral administration induces non-small cell lung cancer cell death

Cocktail of reactive species generated by cold atmospheric plasma: Oral administration induces non-small cell lung cancer cell death

Chang-Hyun Song [1,2§], Pankaj Attri [3§], Sae-Kwang Ku [1,2], Ihn Han [4], Annemie Bogaerts [5] and Eun Ha Choi* [4]

[1] Department of Anatomy and Histology, College of Korean Medicine, Daegu Haany University, Gyeongsan 38610, Korea
[2] Research Center for herbal convergence on liver disease, College of Korean Medicine, Daegu Haany University, Gyeongsan 38610, Korea
[3] Center of Plasma Nano-interface Engineering, Kyushu University, Fukuoka, Japan,
[4] Department of Electrical and Biological Physics, Plasma Bioscience Research Center, Kwangwoon University, Seoul, Korea
[5] Research group PLASMANT, Department of Chemistry, University of Antwerp, BE-2610 Wilrijk-Antwerp, Belgium

Abstract

Non-small cell lung cancer (NSCLC) is the most common type of lung cancer, as 85 % of all lung cancer is reported for NSCLC. Moreover, there are no effective treatments in advanced NSCLC. This study shows the first time that oral administration of plasma-treated water (PTW) can cure advanced NSCLC. The cold plasma in water generates the cocktail of reactive species, and oral administration of this cocktail to mice, showed no toxicities even at the highest dose of PTW, after the single dose and repeated doses for 28 days in mice. *In-vivo* studies reveal that PTW showed favorable anticancer effects on chemo-resistant lung cancer, similarly with gefitinib treatment as a reference drug in chemo-resistant NSCLC model. The anticancer activities of PTW seem to be involved in inhibiting proliferation and angiogenesis and enhancing apoptosis in the cancer cells. Interestingly, the PTW contributes to enhanced immune response and improved cachexia in the model.

Keywords: lung cancer; cold atmospheric plasma; anticancer activities

…….

* Correspondence: ehchoi@kw.ac.kr; § C.H.S. and P.A. share equal contribution

1. Introduction

Lung cancer is the more often cause of cancer-related death, being responsible for about 24 % of total cancer death [1]. Roughly 85 % of the lung cancer are non-small cell lung cancer (NSCLC) with poor prognosis: Five-year survival rate of only 15 % in such patients and less than 3.7 % in the advanced metastatic stages [1]. The histological subtypes include adenocarcinoma, squamous cell lung cancer (SQCLC), and large-cell carcinoma [2]. Since many patients with NSCLC are diagnosed at an advanced stage. The SQCLC, associated strongly with cigarette smoking, is treated mainly using a platinum-based chemotherapy, and median overall survival of the patients in an advanced stage is inferior to one year [3]. Recently, molecular targeting agents, notably epidermal growth factor receptor-tyrosine kinase inhibitors (EGFR-TKIs), have shown significant benefits on the advanced NSCLC, and the first-generation EGFR-TKIs, gefitinib and erlotinib, are approved for treatment of adenocarcinoma harboring EGFR mutations [4]. However, the EGFR-TKIs are effective only in a minority of NSCLC patients with EGFR mutations (8-17% in U.S. and European patients, and fewer in Asian) [5], and they are not sensitive in the patients with wild-type EGFR or a second mutation (i.e. T790M) after treatment with EGFR-TKIs [6]. It suggests there is an urgent need to improve current therapies or develop novel therapeutic concepts for chemo-resistant NSCLC at an advanced stage.

The oxidative mechanism is known to involve pathogenesis of numerous diseases, including lung cancer [7]. Oxidative stress resulting from an imbalance between antioxidant defense abilities and overproduction of oxidants modulates various signaling pathways, causing inflammation, apoptosis, and proliferation [8]. The oxidative stress involves the intracellular reactive oxygen species (ROS) and the free radicals from mitochondria activation or other enzymatic systems, namely NADPH oxidase (NOX), aldehyde oxidase, cytochrome P-450, cyclooxygenase, dihydroorotate dehydrogenase, and nitric oxide synthase (NOS) [9]. Although chronic exposure to low levels of ROS is known to induce tumorigenesis, high levels of ROS have shown cytotoxic effects [10]. Currently, extracellular ROS and reactive nitrogen species (RONS) has shown therapeutic potentials as anti-tumorigenic agents by promoting apoptosis and necrosis, and inhibiting angiogenesis [11], and the various RONS are effective selectively in cancer

cells despite no effects on non-tumor cells [12]. Furthermore, the EGFR-independent antitumor effects of EGFR-TKIs, including gefitinib and erlotinib, have been reported to involve the oxidative stress-mediated pathway [13]. It suggests that oxidative stress overwhelming the antioxidant capacities can be linked to the potential anticancer effects.

Plasma medicine provides a new promising alternative treatment for cancer [14]. To date, irradiation by cold atmospheric plasma has shown dramatic effects on various types of cancer [15–17], and the antitumor effects have also been demonstrated when applying plasma-treated medium (PTM) [16,18,19]. Surya et al. reported that miniature DBD (mDBD) plasma treatment on lung cancer cells results in apoptotic induction and reduces cancer cell migration [20].

Tanaka, et al. demonstrated that PTM could selectively kill glioblastoma (U251SP) cells [21]. Saadati et al. reported that a combination of PTM with chemotherapy could effectively treat tumors more than chemotherapy or PTM alone [22]. Additionally, Utsumi et al. reported the anticancer effect of PTM on chemo-resistant ovarian cancer in both *in vitro and in vivo* studies [23]. Van Boxem et al. revealed that plasma-treated phosphate-buffered saline (PBS) shows a cytotoxic effect on glioblastoma cancer cell lines; additionally, the authors also demonstrated that hydrogen peroxide (H_2O_2) plays a more vital role than nitrite (NO_2^-) in killing cancer cells [18]. Bekeschus et al. reported that plasma-treated PBS significantly decreases pancreatic tumor in a 3D model [24]. Recently, Freund et al. revealed that plasma-treated saline solution treatment was better than H_2O_2 in killing 3D tumor-spheroids grown from murine colon cancer cells [25]. Additionally, *in vivo* studies showed that plasma-treated saline successfully reduced the tumor burden and elevated the immunogenicity [25]. Very recently, Griseti et al. reported that plasma-activated PBS (P-A PBS) was more effective in killing cancer cells of human ovarian cancer and colorectal cancer than plasma-activated sodium chloride 0.9% (P-A NaCl), mainly because higher concentrations of H_2O_2, NO_2^- and nitrate (NO_3^-) were produced in P-A PBS than in P-A NaCl [26]. Yan et al. reported that PTM was highly effective for pancreatic cancer cells, while plasma-treated PBS was more effective for glioblastoma cells. Moreover, the dilution on plasma-treated water (PTW) significantly weakens the anticancer effect on breast cancer cells and pancreatic cancer cells, while dilution did not weaken the toxicity effect against glioblastoma cancer cells [27]. Tanaka,

et al. reported that plasma-activated acetic acid Ringer's solution (PAA) and plasma-activated Ringer's lactate solution (PAL) successfully killed SK-OV-3 cells [28]. Sato et al. showed PAL-induced anticancer effects on pancreatic cancer by *in-vitro* and *in-vivo* studies [17]. In another study, Matsuzaki et al. investigated the PAL-induced anticancer effect on A549 cancer cells [29]. Finally, our and other groups reported the anticancer effect of plasma-treated water (PTW), on human breast cancer cells (MDA-MB-231) [30], on a human cervical cancer cell line (HeLa cell line) [31], and on pancreatic ductal adenocarcinoma (MiaPaca-2, BxPc3) and pancreatic stellate cells (PSCs) (hPSC128-SV) [32].

The oral dose toxicity of PTW was first examined at the maximum dose for rodent, and then the antitumor effects of the orally administered PTW on chemo-resistant NSCLC were examined *in vitro* and *in vivo*. For the antitumor effects, human SQCLC, NCI-H520 that scarcely express EGFR, was used as a gefitinib-resistant NSCLC, and the oxidative stress-mediated antitumor effects of PTW were compared with those of gefitinib treatment [13].

2. Materials and Methods

2.1 Production of PTW

Atmospheric pressure plasma jet comprised of two electrodes and a quartz tube. Hollow needle was used as high voltage electrode and covered with a quartz tube (Figure 1A). The outer electrode acts as the ground electrode. The root-mean-squared voltage and current were 0.58 kV and 2.21 mA, respectively (Figure 1B), whereas the discharge voltage and energy were 1.16 kV and 9.5 mJ/sec, respectively. The relative humidity was 50 % RH. No chemical etching was observed on the walls of the stainless-steel needle after plasma treatment. The optical emission spectra (OES) of the plasma jet emission were recorded using a HR4000CG-UV-NIR spectrometer. Figure 1C, illustrates a typical spectrum, showing that in air plasma small emission lines in the range of 200–250 nm that belongs to the molecular NO β, γ system. Additionally, strong peaks at 294.5, 314.1, 335.3, 353.7, and 379.0 nm were belonging to N_2 second-positive system (C3Πu–B3Πg), as well as $^{\bullet}$OH peak at 309 nm also observed. For PTW, double distilled water (DDW) of 5 ml in a well of 6-well plate was treated with the atmospheric pressure plasma jet for 30 min.

2.2 RONS concentrations and change in pH of PTW

Concentrations of H_2O_2, NO_2^- and NO_3^- in the PTW were measured, as described elsewhere [33–36]. The H_2O_2, NO_2^- and NO_3^- concentrations in the prepared PTW were 0.16 ±0.032, 0.20 ±0.04 and 1.2 ± 0.04 mM, respectively, as shown in Figure 1D. PTW was diluted with DDW for the *in vivo* test and diluted with culture medium RPMI 1640 for the *in vitro* experiments, as shown in Figure 2A, and explained below.

2.3 Animals

Six-week old female and male ICR (CD1®) and five-week old female nude (CAnN.Cg-Foxn1nu/CrljOri) mice were purchased from OrientBio (Seoul, Korea) for studies on oral dose toxicity of PTW and the antitumor effects, respectively. The animals were housed in a temperature (20-25 °C) and humidity (45 %) controlled room with a light/dark cycle of 12 h/12 h. Feed and water were supplied ad libitum. After acclimatization for 7 days at least, animals were used and fasted overnight before the initial treatment and euthanasia with CO_2 gas. All animal experiments were performed according to the guidelines of the international regulations of usage and welfare of laboratory animals, and approved by the Institutional Animal Care and Use Committee in Daegu Haany University (Gyeongsan, Korea) (Approval No. of DHU2016-017 and DHU20160-018 for single and repeated oral dose toxicity of PTW, respectively, and DHU2016-040 for antitumor effects of PTW). PTW was administrated through an oral gavage for both toxicity test (single dose and repeated dose), and antitumor effect.

2.4 Treatment for oral dose toxicity of PTW

Two batches of female and male ICR mice were used for oral dose toxicity of PTW. The experimental procedure for the oral dose toxicity test was demonstrated in Figures S1 and S2. Because no data exists for the toxicity, it was assessed in the maximum oral volume of 20 ml/kg, accepted as a limited dose for rodents by Korea Food and Drug Administration (KFDA) guidelines (Notification No. 2015-082) and as described previously [37–39]. One batch of 40 female and male mice were divided into eight groups with similar body weights (n = 5 per group). The mice received a single oral dose of DW (vehicle control) or PTW at 20, 10 and 5 ml/kg (PTW20, PTW10 and PTW5, respectively) in a volume of 20 ml/kg, as shown in Figure S1. In a same manner, another batch of 40 female and male mice was grouped, and they received the repeated oral dose

for 28 days, see Figure S2. The toxicological analyses were performed according to the KFDA guidelines.

2.5 Single oral dose toxicity of PTW

Abnormal clinical signs and death were recorded twice a day within 14 days post-treatment, based on a functional observation battery [40]. The body weights were measured prior to treatment and on days 1, 2, 7, 13 and 14 post-treatment. On day 14 post-treatment, mice were euthanized and any abnormal changes were scored in the necropsy, especially in specific organs of the brain, lung, heart, liver, thymus, adrenal glands, kidney, spleen, testis/ovary, pancreas, epididymis/uterus, and submandibular lymph nodes, and additional organs of urinary bladder, gastrointestinal tracts, skin, prostate, and the administered sites. The specific organs were sampled and weighted. Then, the samples were fixed in 10 % neutral buffered formalin (NBF), paraffin-embedded, and sectioned at 3-4 μm. The sections were stained with hematoxylin-eosin (HE), and any abnormalities were scored using a computer-based image analysis program (iSolution FL ver 9.1, IMT i-solution Inc., Vancouver, BC, Canada). The necropsy and histopathological abnormalities were scored as +1, +2 and +3 for slight, moderate and severe changes, respectively, by a pathologist blinded to treatment groups [41].

2.6 Repeated oral dose toxicity of PTW

Abnormal clinical signs and death were recorded within 28 days post-treatment in a same manner as described above. Body weights were measured prior to treatment and once a day post-treatment. On day 28 post-treatment, blood samples (0.8-10 ml) were collected into CBC bottles containing EDTA-2K via the inferior vena cava under anesthesia with 3 % isoflurane in a mixture of 70 % N_2O and 28.5 % O_2, and mice were euthanized. The necropsy, specific organ weight and histopathology were performed as described above. For hematology, a portion of blood samples (0.3-0.4 ml) were analyzed using an automated hematology cell counter (Cell-DYN3700, Abbott Laboratories, Abbott Park, IL, USA). The contents included numbers of leukocytes (including neutrophils, eosinophils, basophils, lymphocytes, and monocytes), erythrocytes, platelets, hemoglobin concentrations, hematocrit, mean corpuscular volume, mean corpuscular hemoglobin, and mean corpuscular hemoglobin concentration. For serum biochemistry, the rest of blood samples was centrifuged at 3,000 rpm for 10 min, and the resultant serum (about 0.3 ml) was analyzed using a blood biochemistry autoanalyzer (Dri-Chem

NX500i, Fuji Medical System Co., Ltd., Tokyo, Japan). The contents included alkaline phosphatase, aspartate aminotransferase, alanine aminotransferase, blood urea nitrogen, glucose, inorganic phosphorus, albumin, cholesterol, creatine phosphokinase, creatinine, total bilirubin and protein, globulin, albumin/globulin ratio, triglyceride, lactate dehydrogenase, and ions of calcium, sodium, potassium and chloride.

2.7 Antitumor effects of PTW

2.7.1. Human NSCLC cell culture

Human NCI-H520 (American Type Culture Collection, Manassas, VA, USA) cells were maintained in RPMI 1640 media (Gibco BRL, Grand Island. NY, USA) supplemented with 10 % fetal bovine serum (Gibco BRL), 100 U/ml penicillin/streptomycin (Sigma-Aldrich) at 37 °C in a humid atmosphere with 5% CO_2.

2.7.2. In-vitro MTT assay

NCI-H520 cells (1×10^4 cells/well) were plated in 96-well plates and treated with PTW and gefitinib. PTW was 10 times diluted in culture medium and added to the cells at 0, 5, 10, 20, 50, and 100 μl/ml. The same was true for gefitinib at 0, 1, 2.5, 5, 10, and 50 μM, keeping the total volume of 200 μl for 72 hrs. After incubation with 0.5 mg/ml MTT solution (Sigma-Aldrich) for 4 h, the culture medium was changed to DMSO (Sigma-Aldrich). The optical density was measured at 570 nm using a microplate reader (Tecan, Männedorf, Switzerland). Six independent assays were conducted.

2.7.3 Experimental design in NSCLC xenograft model

A total of 48 nude mice were divided into six groups (n = 8 per group) based on similar body weights. The experimental procedure to study the anticancer effect of PTW was shown in Figure 2B. Five groups were inoculated subcutaneously with NCI-H520 cells (2×10^7 cell/mouse) suspended in saline on the right dorsal hip for tumor-bearing (TB) model, while one group was inoculated with saline only. Two weeks later, the TB model was regrouped with similar variability of tumor volumes (a range of 167.47 ~ 479.23 mm^3), and orally administered with DW (TB control), geftinib at 120 mg/kg or PTW at 2.0, 1.0 and 0.5 ml/kg (PTW2.0, PTW1.0 and PTW0.5, respectively) using an oral gavage. Another one group with saline only was administered with DW (Intact). The highest dosage of PTW was determined as a general safety index (10 %) of the maximum dosage (20 ml/kg) in the toxicity studies, and gefitinib was based on a previous study

[42]. The administration was performed in a volume of 10 ml/kg once a day for 35 days. Body weights and tumor volumes were measured prior to treatment and on days 1, 3, 7, 14, 21, 28, and 34 post-treatment. The tumor volumes were calculated with following formula [43]:

$$\text{Tumor volume } (mm^3) = (a \times b^2)/2 \qquad (1)$$

where a is the tumor length (long axis) and b is the tumor width (short axis).

On day 35 post-treatment, the blood was sampled, and mice were euthanized. The tumor mass, three organs of the spleen, the left submandibular lymph nodes and periovarian fat tissues were sampled and weighted. The organ weight to the individual body weight was expressed as the relative weights (%). In addition, the peritoneal lavages were collected. The samples were subjected to biochemical or histopathological analyses.

2.7.4 Serum levels of interleukin (IL)-6 and interferon (IFN)-γ

A blood sample via vena cava was collected before euthanasia, and the serum was separated. The serum sample was stored −150 °C until analysis. The serum levels of IL-6 and IFN-γ were assessed using the IL-6 (R&D Systems Inc., Minneapolis, MN, USA) and the IFN-γ enzyme-linked immunosorbent assay (ELISA) kits (BD Biosciences/Pharmingen, San Jose, CA, USA), respectively, according to the manufacturer's protocols, and expressed as pg/ml.

2.7.5 Natural killer (NK) cell activities

The splenic and peritoneal NK cell activities were assessed by a standard chromium (^{51}Cr) assay, as described previously [44–46]. Briefly, RBC-free splenocytes and peritoneal macrophages as effector cells were isolated from the spleen homogenates and peritoneal lavages, respectively. They were incubated with Na251CrO4-labeled HTLA-230 neuroblastoma target cells (1×10^6 cells) for 6 h at 37 °C. The ratio of effector cells to target cells was 100:1 for splenocytes and 10:1 for peritoneal macrophages. The ^{51}Cr releases were measured in the supernatants using a gamma counter (Cobra 5002; Canberra Packard, Meriden, CT, USA), and calculated with the following formula:

$$\%\ ^{51}Cr \text{ release (NK cell activities)} = [(Exp - S)/(M - S)] \times 100$$

where Exp is the mean ^{51}Cr value observed in the experimental group, S is the mean spontaneous ^{51}Cr value, and M is the mean maximum ^{51}Cr value.

2.7.6 Splenic cytokine measurements

Contents of TNF-α, IL-1β, and IL-10 in the splenic homogenates were measured using the mouse ELISA kits for TNF-α (BD Biosciences/Pharmingen, San Jose, CA, USA), IL-1β (Genzyme, Westborough, MA, USA) and IL-10 (Genzyme, Westborough, MA, USA), respectively, as described previously [47]. The values are expressed as pg/mg tissue protein.

2.7.7 Histopathology

Tissue samples were fixed in 10% NBF, paraffin-embedded and serial-sectioned at a thickness of 3 μm. The sections were stained with HE, and analyzed by a histopathologist blinded to the groups, using a computer-based automated image analyzer (iSolution FL ver 9.1, IMT i-solution Inc.) under microscopy [48,49]. The tumor mass, tumor volumes and apoptotic cells were assessed. The spleen was examined for the thickness of the central region of the spleen, the white pulp numbers and diameters, and the submandibular lymph node were examined for thickness of the central region, cortex lymphoid follicles and cortex thicknesses. The periovarian fat pad was examined for thicknesses of the central region and diameter of white adipocytes.

2.7.8 Immunohistochemistry

The other serial sections were immunostained after antigen retrieval pretreatment in citrate buffer, as described previously [50]. Briefly, endogenous peroxidase was inactivated with 0.3 % H_2O_2, and non-specific immunoglobulin was blocked with normal horse serum solution. A total of 8 primary antibodies was used for the immunostains; 6 rabbit antibodies were used for cleaved caspase-3 (#9661, Cell signaling Technology, Beverly, MA, USA, dilution of 1:400), PARP (#9545, Cell signaling Technology, dilution of 1:100), NT (#06-284, Millipore, Temecula, CA, USA, dilution of 1:200), 4HNE (#ab46545, Abcam, Cambridge, UK, dilution of 1:200), Ki-67 (#ab16667, Abcam, dilution of 1:100), and iNOS (#sc-651, Santa Cruz Biotechnology, Santa Cruz, CA, USA, dilution of 1:100), while 2 rat and mouse monoclonal antibodies were used for CD31 (#550274, BD Bioscience, San Jose, CA, USA, dilution of 1:100) and TNF-α (#sc-130349, Santa Cruz Biotechnology, dilution of 1:200), respectively. The immunoreactivities were biotinylated and visualized using the Vectastain Elite ABC Kit™ and the DAB Peroxidase Substrate Kit™ (Vector Lab. Inc., Burlingame, CA, USA),

respectively. Cells that occupied over 20% of the immunoreactivities were regarded as positive.

2.8 Statistical analyses

The values were expressed as the mean ± standard deviation (S.D.). Firstly, the homogeneity of the variance was analyzed by the Levene test. If the test indicated no significance, the data were analyzed by ANOVA, followed by Scheffe or least-significant differences (LSD) post-hoc tests. However, in case of significance, the Kruskal-Wallis H test was conducted for non-parametric comparison, followed by the Mann-Whitney U (MW) post-hoc test. The data for kinetics changes on body weight and tumor volumes were examined by two-way ANOVA with main factors for the groups and day measured, and the days were treated as a repeated measurement. The value of IC_{50} was calculated by the Probit method. Statistical significance was defined as $p<0.05$ for all analyses.

3. Results

3.1 Oral dose toxicity of PTW in mice

Within 14 days after single dosing, there were no PTW-related mortalities, body weight changes and abnormal clinical signs in both female and male mice administered with PTW at three doses of 20, 10 and 5 ml/kg (PTW20, PTW10 and PTW5, respectively) compared with the vehicle (distilled water, DW) control. Although post-mortem examination of necropsy, specific organ weights and histopathology showed slight abnormal changes, including the lung congestion, hypertrophy in the lymph node and spleen, and the thymic atrophy, the changes were observed either in both vehicle control and PTW groups or in the PTW-dose independent manner. The details are described in the supporting information (Table S1). This supports little potential toxicity of PTW even at the maximum dose of 20 ml/kg via oral administration. The PTW toxicity was further examined in both genders of mice by the repeated oral dosing for 28 days. No mortalities, body weight changes and abnormal signs were observed in all PTW groups. Similar with the single oral dose, the hematology, serum biochemistry and post-mortem examination showed some slight abnormal changes, however, the changes were observed either in both vehicle control and PTW groups or PTW-dose independent manner. The PTW-

specific changes were observed in the weight of liver of PTW20 with 5% increase comparing to the vehicle control. In addition, the splenic hypertrophy was evident dose-dependently in the PTW groups despites no increases in the spleen weights. However, it is unlikely that the results could be involved in the PTW-specific toxicity because of no histopathological abnormalities. The details are also described in the supporting information (Table S2 and Table S3). These indicate that the maximum tolerable dosages in the repeated oral dosing can be over 20 ml/kg in both female and male mice.

3.2. Antitumor effects of PTW in vitro

The cell viability of NCI-H520 was analyzed using different dilutions of PTW and gefitinib. A similar drop in cell viability upon rising concentration was observed, and the gradient showing the dose-dependent cell death was even more pronounced for PTW than for gefitinib. IC_{50} of 9.73 ±0.87 μl/ml was obtained in PTW treatment, and 4.98 ±0.69 μM in gefitinib (Figures 3A and 3B). The probable mechanism of PTW action on cancer cells was discussed in discussion section and shown in Figure 3C.

3.3 Antitumor effects of PTW

In NSCLC xenograft model, while the inoculated tumor was grossly grown in the tumor-bearing (TB) vehicle-treated control group for 35 days, it was little grown in the PTW and gefitinib groups. The kinetic changes of the body weight and the tumor growth were examined by two-way ANOVA (Figure 4). For the body weight changes, there were no significant effects for the group, but significant interactions between the group and days ($p<0.01$). The post hoc tests versus the TB control revealed a significant body weight loss in the gefitinib group on days 21 to 35 post-treatment (Figure 4A). Although the TB control exhibited the cachexia, the body weights including a huge tumor mass showed no significances compared to the PTW groups. For the tumor size, there were substantial effects of the groups ($p<0.01$), and interactions between group and days ($p<0.01$). The post hoc tests versus the TB control revealed significant inhibition of tumor growth in the PTW2.0, PTW1.0 and gefitinib groups on days 7 to 35 post-treatment and in the PTW0.5 on days 14 to 35 ($p<0.05$, Figure 4B). After all treatment for 35 days, the exposed tumor was relatively smaller in the PTW groups, especially PTW2.0 and gefitinib than the TB control (Figure 4C). The relative weights versus the TB control were lower by 63.4%, 51.8%, 35.8% and 52.8%, in the PTW2.0, PTW1.0, PTW0.5 and gefitinib groups,

respectively. As expected, the body weight subtracted from the tumor weight showed considerable increases of the weight gains in the groups of PTW2.0 and PTW1.0 compared with the TB control ($p<0.05$), while it showed a decrease in the gefitinib group ($p<0.01$, Figure 4D). Additionally, the absolute and relative tumor weights showed significant reduction in the PTW and gefitinib groups compared with the TB control ($p<0.01$, Figures 4E and 4F).

3.4 Effects on immune-relative organs and cachexia

We assessed the weights of the spleen and lymph node for immune responses in the TB model, and the periovarian fat tissues for the cachexia. The TB control group exhibited a significant reduction in the absolute and relative weights of the spleen, lymph node and fat tissues, compared with those of the intact group (Table S4). However, comparing to the TB control, the absolute and relative weights were significantly increased in the PTW groups ($p<0.05$), but not in the gefitinib. The relative weights versus the TB control were increased by 1.5-, 1.3- and 1.2-folds in the spleen of the PTW2.0, PTW1.0 and PTW0.5 groups, respectively. Likewise, they were increased by 2.4-, 1.8-, and 1.7-folds in the lymph node, and by 2.6-, 2.1-, and 1.8-folds in the fat tissues.

3.5 Effects on cytokines and natural killer (NK) cell activities

Serum levels of interferon (IFN)-γ and interleukin (IL)-6, and the splenic levels of tumor necrosis factor (TNF)-α, IL-1 and IL-10 were further assessed for the TB-relevant immune responses (Figures 5A and 5B). The TB control group versus the intact group showed notable increases in the serum levels of IL-6 and decreases in the levels of IFN-γ, however, all PTW groups versus the TB control reversed the serum levels. In addition, the splenic levels of TNF-α, IL-1 and IL-10 were decreased in the TB control compared with the intact group ($p<0.01$), however, they were significantly increased in the PTW groups comparison with the TB control ($p<0.01$). There were no differences in the serum and splenic cytokine levels between the TB control and gefitinib groups. Corresponding to the cytokines, the TB control group showed a significant decrease in the splenic and peritoneal NK cell activities comparing with the intact group ($p<0.01$, Figure 5C), however, the PTW groups showed a significant increase in the activities comparing to the TB control group ($p<0.01$). No differences were found in the activities between the TB control and gefitinib groups.

3.6 Histopathological changes on tumor mass

The TB control group exhibited well-differentiated tumor cells as squamous carcinoma with a relatively fewer apoptotic cells in the xenograft tumor mass (Figure 6A). In the PTW and gefitinib groups, on the other hand, the tumor cells were evidently reduced. The histomorphometric analysis revealed significant decreases in tumor cells by 49.9%, 57.4%, 78.5%, and 59.6% in the PTW2.0, PTW1.0, PTW0.5 and gefitinib groups, respectively ($p<0.01$, Figure 6B). Regarding the reduced tumor cells, the cell apoptosis and proliferation in the tumor mass were analyzed (Figure 7A). The immunoreactive cells for caspase-3 and poly (ADP-ribose) polymerase (PARP) as apoptosis makers were observed more in the PTW and gefitinib groups than the TB control. Vice versa, the immunoreactive cells for Ki-67 as a proliferation marker were observed fewer in the PTW and gefitinib groups. The histmorphometric analysis revealed significant increases in the immunoreactive cells for caspase-3 and PARP in the PTW (especially PTW2.0) and gefitinib groups, compared with the TB control group, and significant decreases in the cells for Ki-67 ($p<0.01$, Figures 7B and 7C). Angiogenesis in the stroma was assessed in immunostain for cluster of differentiation (CD)31, and the immunoreactive cells were significantly decreased in the PTW and gefitinib groups, compared with the TB control ($p<0.01$). For further mechanisms, nitrotyrosine (NT) and 4-hydroxynonenal (4HNE) were immunostained for oxidative stress, and inducible nitric oxide synthases (iNOS) and tumor necrosis factor (TNF)-α were for immune activities. The immunoreactive cells were observed evidently more in the PTW groups than the TB control. The histomophometric analyses revealed significant rise in the immunoreactive cells for NT, 4HNE, iNOS and TNF-α in the PTW groups compared with the TB control ($p<0.01$, Figures 7D and 7E). The gefitinib group also showed increases in the immunoreactive cells for NT, 4HNE, and TNF-α, but not for iNOS.

3.7 Histopathological changes on immune organ and fat tissues

The TB control group exhibited atrophic changes with reduced lymphoid cells in the splenic white pulp and lymph nodes (Figure 8). In addition, noticeable atrophic changes with reduced volumes and numbers of white adipocytes in the periovarian fat tissues were observed. The atrophic changes seemed to be improved in the PTW groups, but not in the gefitinib group. The histomorphometric analyses revealed major decreases in the splenic thickness and its white pulp numbers and diameters in the TB control group compared with the intact group, together with decreases in the lymph node thickness, the lymphoid

follicles and the cortical thickness ($p<0.01$) (Table 1). Furthermore, also the thickness of the fat tissues reduced significantly, with reduced diameters of adipocytes ($p<0.01$). Interestingly, the reduced parameters in the spleen, lymph node and fat tissues were substantially increased in the PTW groups compared with the TB control group, but not for the gefitinib group ($p<0.01$).

3. Discussion

Since this is the first study on oral dose toxicity of PTW in mice, the toxicological profiles were examined at the limited dosage for rodents and sequentially diluted dosages. The single oral dose of PTW showed no mortalities in both genders of mice up to 14 days post-treatment, and no differences in the clinical signs and body weight changes compared with the vehicle control group. Likewise, no PTW-specific abnormalities were found in the necropsy, organ weight and histopathological analyses although there were some sporadic changes. The same was observed even by repeated dose of PTW for 28 days, with no mortalities in both genders and no PTW-specific abnormalities in the gross examination and blood analyses. The serum albumin and bilirubin are known to be strong antioxidant elements [51], however, they were not different in the PTW groups compared with the control. It suggests the total antioxidant defense system in normal condition counteract sufficiently the oxidative stress induced by the PTW. The histopathological examination revealed little abnormalities in most of the organs, but the spleen showed the PTW-specific hypertrophy in the red pulp with the lymphoid cells' hyperplasia. It is unclear how PTW reacts with the splenic immune cells. However, considering that there were no differences in weights of 14 specific organ including the spleen along with no abnormal lesions, the splenic hypertrophy was probably due to immune responses stimulated by PTW, rather than its toxicity [52]. These support that PTW can be applied orally even at the maximum dosage for rodents, suggesting possibilities for a clinical use of PTW via an oral route.

EGFR-TKIs have favored in adenocarcinomas with EGFR mutations. However, they are effective only in a minority of NSCLC patients, and NSCLCs with wild-type EGFR or negative EGFR are considered to be resistant to the EGFR-TKIs. Here, the gefitinib exhibits IC_{50} of high dose in the NCI-H520 negative EGFR cells similar with other studies [5,53]. The cell viability assay provided a direct evidence for anti-proliferative effects of

PTW on NSCLC. The gradient of inhibition curve seemed to be more pronounced in the PTW treatment than the gefitinib, suggesting high sensitivity to PTW in the EGFR-TKI-resistant NSCLC. In addition, the oral administration of PTW inhibited progressive tumor growth showing reduction of tumor size and weights in the NSCLC xenograft mice model. It is enigmatic regarding about the selective cytotoxicity of PTW on tumor cells and the systemic antitumor effects. The levels of oxidative stress increase in advanced stages of lung cancer, through the oncogene activation and the subsequent cellular metabolisms, while levels of the antioxidant molecules decrease [54]. So, we speculated the selective cytotoxicity was probably due to inability of antioxidant defense system in cope with the extrinsic RONS in PTW in addition to higher basal ROS levels in tumor cells than normal cells. The systemic antitumor effects of PTW are more difficult to interpret because the only small amounts of RONS in the administered PTW are expected to reach to the tumors through the gastrointestinal tract. Future studies on the serum levels of RONS including H_2O_2, NO_2^- and NO_3^- need to be clarified for the direct antitumor effects of PTW via an oral route. However, the data of immunostains for caspase-3, PARP, Ki-67 and CD31 supported further the antitumor effects of PTW by enhancing apoptosis and inhibiting cellular proliferation and stromal angiogenesis in the tumor mass.

Excessive oxidative stress over antioxidant mechanisms in tumor itself symbolize as an alternative and promising therapeutic options for tumors refractory to the treatment for NSCLC [55,56]. The present results in the immunostains for NT and 4HNE represented significant increases in the oxidative stress in the PTW groups as well as the geftinib compared with the TB control. The EGFR-independent antitumor effects involved in oxidative stress have been reported recently [13]. In this text, we used a gefitinib as a reference drug for the oxidative stress-meditated antitumor effects comparing to PTW in chemo-resistant NSCLC. Gefitinib induces a dose-dependent increase of oxidative stress-mediated cytotoxicity [57]. In contrast, elevated expression of peroxiredoxins (Prx) II, an antioxidant, involves gefitinib-resistant tumor cells, and inhibition of the antioxidants by down-regulation of Prx II or inactivation of nuclear factor erythroid 2-related factor 2, a major antioxidant response regulator, enhances the antitumor effects of EGFR-TKIs. However, the EGFR-mediated signaling pathway seems to have dual effects depending on the degree of oxidative stress: While oxidation of wild-type EGFR induces ROS generation and EGFR activation, leading to the

downstream signaling pathways to promote tumorigenesis [58], high levels of oxidative stress may induce the EGFR degradation or inactivation [59]. Indeed, a ROS producer like sanguinarine and overproduction of ROS through superoxide and hydrogen peroxide production causes EGFR degradation and then cell death even in EGFR-TKIs-resistant NSCLC [60,61]. Besides, reagents such as piperlongumine and shikonin, elevating ROS, have shown antitumor properties with enhancing apoptosis and inhibiting angiogenesis. The increased RONS exerted endoplasmic reticulum stress and unfolded protein response activation, which induces mitochondria-mediated apoptosis by triggering PERK-dependent activation of JNK and p38 MAPK [62,63].

Interestingly, the systemic effects of PTW resulted in an improvement of the cachexia by inhibition of weight loss and decreased fatty tissue. Pathogenesis and progression of cachexia have been attributed in part to systemic elevation of pro-inflammatory cytokine [64], while the resulting cachexia induces a suppressive effect on T cell-mediated anticancer immune reaction [65]. Although nude mice are congenitally athymic for T lymphocyte-related immune deficiency [66], they develop the extra-thymic T cell maturation with CD8+ cytotoxic T cells more than CD4+ helper T cells [67]. Here, the TB control group exhibited remarkable weight loss, along with the reduced weights of the immune organs, including the spleen and submandibular lymph node. It was accompanied by the elevated serum levels of IL-6, observed mainly in patients with cachexia-associated cancers [68], and the reduced levels of IFN-γ and splenic TNF-α, IL-1β and IL-10, related to immune response. Vice versa, the PTW inhibited the cachexia by reducing the IL-6 levels and increasing the weights of immune organs and releases of the relevant cytokines. The histopathological analyses supported for the improvement of cachexia in the PTW treatment showing the reduced atrophic changes in the spleen and lymph nodes and the increased expression of iNOS and TNF-α in the tumor mass. The enhanced immune responses in the PTW groups might be linked to the significant increases in the splenic and peritoneal NK cells, contributing to the antitumor effects and then improving the cachexia. Together with splenic hypertrophy in the above toxicological studies, the results suggest that the antitumor effects of PTW may be mediated through the immune stimulation involved in the oxidative stress [42]. However, the cachexia and immune responses were not different in the gefitinib group compared with the TB control despite significant inhibition of tumor growth. Cachexia in lung

cancer patients receiving gefitinib or other cytotoxic reagents has been an issue, because the therapies are focused typically on reducing tumor mass [69]. We expect that PTW can overcome this drawback and cure cancer in a better way.

Oxidative stress-regulated reduction-oxidation reaction (redox) signaling pathways are involved in cancer progression, especially in SQCLC associated with cigarette smoking. However, clinical trials using antioxidants (i.e. vitamin, A, C and E, retinol and beta-carotene) have no significant impacts or rather increase incidences of certain cancers, including lung cancers [70]. It suggests the establishment of novel therapeutic strategies using oxidative stress-mediated mechanisms for the treatment of the refractory NSCLC. There have been currently emerging potential molecular targets as anaplastic lymphoma kinase, BRAF, PDGFR and VEGFR as well as EGFR, for NSCLC, which has also shown antitumor properties via increased oxidative stress as well as their targeted impacts [13]. To understand the concrete action of PTW on the tumor through oral administration in mice is not straightforward because of the complex system due to the buffering capacity of the stomach and gastrointestinal tract.

The chemical composition of PTW (H_2O_2, NO_2^- and NO_3^-) initiates the redox biochemistry, so we speculate which could be the relevant pathways for cancer cell death, as described in Figure 3C, based on literature. It is generally accepted that the intracellular ROS concentration increases after plasma treatment due to an increased influx of extracellular RONS into the cells [32,71–76]. The extracellular RONS produced in PTW undergo multiple reactions, as listed below [77], which play an essential role in cancer cell death through oxidative stress.

$NO_2^- + H_2O_2 \longrightarrow ONOO^- + H_2O$ (1)

$H^+ + ONOO^- \longrightarrow ONOOH$ (2)

$ONOOH \longrightarrow {}^\bullet NO_2 + {}^\bullet OH$ (3)

$ONOO^- + H_2O_2 \longrightarrow {}^1O_2 + H_2O + NO_2^-$ (4)

$H_2O_2 + {}^\bullet OH \longrightarrow H_2O + HO_2^\bullet$ (5)

$HO_2^\bullet + O_2^{\bullet-} + H^+ \longrightarrow {}^1O_2 + H_2O_2$ (6)

l-arginine + NOS $\longrightarrow$ l-citrulline + $NO^\bullet$ (7)

$O_2^{\bullet-} + NO^\bullet \longrightarrow ONOO^-$ (8)

~~H_2O_2 + catalase $\longrightarrow$ H_2O + 1/2 O_2~~ (9)

~~$ONOO^-$ + catalase $\longrightarrow$ NO_2^- + 1/2 O_2~~ (10)

It was reported that extracellular RONS can trigger membrane-associated intracellular signaling, which results in cell death [78]. As seen from our chemical analysis, PTW comprises H_2O_2 and NO_2^- (next to NO_3^-), and these species are long-lived, so they are stable in PTW. The reaction between H_2O_2 and NO_2^- generates $ONOO^-$ (eq. 1) (see Figure 3C). Subsequently, protons derived from the membrane-associated proton pump react with $ONOO^-$ to generate ONOOH (eq. 2). ONOOH decomposes to ${}^\bullet NO_2$ and ${}^\bullet OH$ (eq. 3). Another possibility is that $ONOO^-$ reacts with H_2O_2 to form ${}^1O_2$ (eq. 4). Subsequently, ${}^\bullet OH$ reacts with H_2O_2 to form $HO_2^\bullet$ (eq. 5), and $HO_2^\bullet$ reacts with $O_2^{\bullet-}$ (generated by NOX enzyme) into ${}^1O_2$ (eq. 6). ${}^1O_2$ produced from eq. 4 and 6 either activates the FAS receptor (ligand independent pathway) [79] or deactivates catalase through reaction with histidine (active site of catalase) [80,81] or a combination of both. The FAS receptor activation results in FAS-associated death domain protein (FADD) activation, which activates caspase-8, followed by NOS and NOX activity [77]. The activation of caspase-8 activates capase-3 and later PARP, which results in cell death [82]. This is one pathway that may occur in our system.

Another possible pathway is that the enhancement of NOS (Figure 7F also shows high iNOS generation after PTW treatment) and NOX generates $NO^\bullet$ (eq. 7). The latter reacts with $O_2^{\bullet-}$, to form $ONOO^-$ (eq. 8). Hence, the concentration of $ONOO^-$ increases, as it is generated by eqs. 1 and 8, and through eq. 4 it generates ${}^1O_2$. Hence, we expect

the concentration of $^1O_2$ to increase in our system, directly related to catalase inactivation (Figure 3C).

As more catalase enzyme is deactivated, H_2O_2 and $ONOO^-$ will not be converted into H_2O and NO_2^-, respectively, by eqs 9 and 10 (hence the cross through these reactions). So, the available H_2O_2 enters the cell, e.g., through aquaporin [83], to increase the intracellular ROS concentration. Furthermore, the available $ONOO^-$ converts to $^{\bullet}OH$ by eqs 2 and 3. The $^{\bullet}OH$ reacts with the cell membrane lipids, resulting in lipid peroxidation, which triggers a cell death pathway [84]. Additionally, the antioxidant mechanisms will fail inside the cell due to the excess intracellular RONS concentration, which results in DNA damage and leads to cell death, as displayed in Figure 3C. However, more research will be needed to elucidate the exact mechanisms and specify the role of other antioxidant defense mechanisms, which are not yet included in the present hypothesis.

5. Conclusions

For the first time, we have presented the systemic application of PTW to treat lung cancer via oral administration. We demonstrated that both single and repeated oral doses of PTW could be non-toxic in the maximum volume for rodents, suggesting safety for clinical use. Furthermore, no specific target or clinical signs were detected after oral administration of PTW. Further, the oral administration of PTW showed favorable anticancer activities through oxidative stress to the implanted tumor cells in the mice. PTW treatment inhibited proliferation and angiogenesis. Interestingly, PTW showed a clear improvement of cachexia and immunostimulation, unlike the chemotherapeutic drug, gefitinib. In a further study, we should evaluate the long-term effects of PTW for the treatment of NSCLC and the relevant mechanisms.

Ethical Statement: This study was carried out according to the methods described in the Testing Guidelines for Safety Evaluation of Drugs (Notification No. 2015-082, 2015) issued by the Korea Food and Drug Administration (KFDA) on November 11, 2015. In addition, this animal experiment was conducted according to the international regulations of the usage and welfare of laboratory animals, and approved by the Institutional Animal Care and Use Committee in Daegu Haany University (Gyeongsan, Korea) [Approval No. DHU2016-017. March 04. 2016; ANNEX III].

Data Availability: All data supporting data is present in the supporting information file.

Author Contributions: C.H.S. and E.H.C. designed the experiment. C.H.S. and S.K.K. performed the animal experiments. I.H performed the immunostained for CD31. P.A., A.B. and E.H.C. performed the plasma experiments and standardize the conditions. C.H.S wrote the main draft of manuscript. P.A., A.B., and C.H.S revised the manuscript.

Funding: We gratefully acknowledge financial support from Leading Foreign Research Institute Recruitment program (Grant # NRF-2016K1A4A3914113) through the Basic Science Research Program of the National Research Foundation (NRF) of Korea and in part by Kwangwoon University.

Conflicts of Interest: The authors declare that they have no competing interests.

References

[1] Siegel R L, Miller K D and Jemal A 2016 Cancer statistics, 2016 *CA. Cancer J. Clin.* **66** 7–30

[2] Drilon A, Rekhtman N, Ladanyi M and Paik P 2012 Squamous-cell carcinomas of the lung: emerging biology, controversies, and the promise of targeted therapy *Lancet Oncol.* **13** e418–26

[3] Bonanno L 2013 Predictive models for customizing chemotherapy in advanced non-small cell lung cancer (NSCLC). *Transl. lung cancer Res.* **2** 160–71

[4] Janku F, Garrido-Laguna I, Petruzelka L B, Stewart D J and Kurzrock R 2011 Novel Therapeutic Targets in Non-small Cell Lung Cancer *J. Thorac. Oncol.* **6** 1601–12

[5] Helfrich B A, Raben D, Varella-Garcia M, Gustafson D, Chan D C, Bemis L, Coldren C, Baron A, Zeng C, Franklin W A, Hirsch F R, Gazdar A, Minna J and Bunn P A 2006 Antitumor Activity of the Epidermal Growth Factor Receptor (EGFR) Tyrosine Kinase Inhibitor Gefitinib (ZD1839, Iressa) in Non-Small Cell Lung Cancer Cell Lines Correlates with Gene Copy Number and EGFR Mutations but not EGFR Protein Levels *Clin. Cancer Res.* **12** 7117–25

[6] Masters G A, Temin S, Azzoli C G, Giaccone G, Baker S, Brahmer J R, Ellis P M, Gajra A, Rackear N, Schiller J H, Smith T J, Strawn J R, Trent D, Johnson D H and American Society of Clinical Oncology Clinical Practice 2015 Systemic Therapy for Stage IV Non–Small-Cell Lung Cancer: American Society of Clinical Oncology Clinical Practice Guideline Update *J. Clin. Oncol.* **33** 3488–515

[7] Masri F 2010 Role of nitric oxide and its metabolites as potential markers in lung cancer *Ann. Thorac. Med.* **5** 123

[8] Kousteni S 2011 FoxOs: Unifying links between oxidative stress and skeletal homeostasis *Curr. Osteoporos. Rep.* **9** 60–6

[9] Filaire E, Dupuis C, Galvaing G, Aubreton S, Laurent H, Richard R and Filaire M 2013 Lung cancer: What are the links with oxidative stress, physical activity and nutrition *Lung Cancer* **82** 383–9

[10] Valko M, Rhodes C J, Moncol J, Izakovic M and Mazur M 2006 Free radicals, metals and antioxidants in oxidative stress-induced cancer *Chem. Biol. Interact.* **160** 1–40

[11] Halliwell B and Gutteridge J M C 2015 *Free Radicals in Biology and Medicine* (Oxford University Press)

[12] Chen Q, Espey M G, Sun A Y, Lee J-H, Krishna M C, Shacter E, Choyke P L, Pooput C, Kirk K L, Buettner G R and Levine M 2007 Ascorbate in pharmacologic concentrations selectively generates ascorbate radical and hydrogen peroxide in extracellular fluid in vivo *Proc. Natl. Acad. Sci.* **104** 8749–54

[13] Teppo H-R, Soini Y and Karihtala P 2017 Reactive Oxygen Species-Mediated Mechanisms of Action of Targeted Cancer Therapy *Oxid. Med. Cell. Longev.* **2017** 1–11

[14] Hirst A M, Frame F M, Arya M, Maitland N J and O'Connell D 2016 Low temperature plasmas as emerging cancer therapeutics: the state of play and thoughts for the future *Tumor Biol.* **37** 7021–31

[15] Attri P, Kumar N, Park J H, Yadav D K, Choi S, Uhm H S, Kim I T, Choi E H and Lee W 2015 Influence of reactive species on the modification of biomolecules generated from the soft plasma *Sci. Rep.* **5** 8221

[16] Attri P, Park J H, Ali A and Choi E H 2018 How Does Plasma Activated Media Treatment Differ From Direct Cold Plasma Treatment? *Anticancer. Agents Med. Chem.* **18** 805–14

[17] Sato Y, Yamada S, Takeda S, Hattori N, Nakamura K, Tanaka H, Mizuno M, Hori M and Kodera Y 2018 Effect of Plasma-Activated Lactated Ringer's Solution on Pancreatic Cancer Cells In Vitro and In Vivo *Ann. Surg. Oncol.* **25** 299–307

[18] Van Boxem W, Van der Paal J, Gorbanev Y, Vanuytsel S, Smits E, Dewilde S and Bogaerts A 2017 Anti-cancer capacity of plasma-treated PBS: effect of chemical composition on cancer cell cytotoxicity *Sci. Rep.* **7** 16478

[19] Kumar N, Park J H, Jeon S N, Park B S, Choi E H and Attri P 2016 The action of microsecond-pulsed plasma-activated media on the inactivation of human lung cancer cells *J. Phys. D. Appl. Phys.* **49** 115401

[20] Karki S B, Yildirim-Ayan E, Eisenmann K M and Ayan H 2017 Miniature Dielectric Barrier Discharge Nonthermal Plasma Induces Apoptosis in Lung Cancer Cells and Inhibits Cell Migration *Biomed Res. Int.*

[21] Tanaka H, Mizuno M, Ishikawa K, Nakamura K, Kajiyama H, Kano H, Kikkawa F and Hori M 2011 Plasma-activated medium selectively kills glioblastoma brain tumor cells by down-regulating a survival signaling molecule, AKT kinase *Plasma Med.* **1** 265–77

[22] Saadati F, Mahdikia H, Abbaszadeh H-A, Abdollahifar M-A, Khoramgah M S and Shokri B 2018 Comparison of Direct and Indirect cold atmospheric-pressure plasma methods in the B16F10 melanoma cancer cells treatment *Sci. Rep.* **8** 7689

[23] Utsumi F, Kajiyama H, Nakamura K, Tanaka H, Mizuno M, Ishikawa K, Kondo H, Kano H, Hori M and Kikkawa F 2013 Effect of Indirect Nonequilibrium Atmospheric Pressure Plasma on Anti-Proliferative Activity against Chronic Chemo-Resistant Ovarian Cancer Cells In Vitro and In Vivo ed M Yousfi *PLoS One* **8** e81576

[24] Bekeschus S, Käding A, Schröder T, Wende K, Hackbarth C, Liedtke K R, van der Linde J, von Woedtke T, Heidecke C-D and Partecke L-I 2018 Cold Physical Plasma-Treated Buffered Saline Solution as Effective Agent Against Pancreatic Cancer Cells *Anticancer. Agents Med. Chem.* **18** 824–31

[25] Freund E, Liedtke K R, van der Linde J, Metelmann H-R, Heidecke C-D, Partecke L-I and Bekeschus S 2019 Physical plasma-treated saline promotes an immunogenic phenotype in CT26 colon cancer cells in vitro and in vivo *Sci. Rep.* **9** 634

[26] Griseti E, Merbahi N and Golzio M 2020 Anti-cancer potential of two plasma-activated liquids: Implication of long-lived reactive oxygen and nitrogen species *Cancers (Basel).*

[27] Yan D, Cui H, Zhu W, Nourmohammadi N, Milberg J, Zhang L G, Sherman J H and Keidar M 2017 The Specific Vulnerabilities of Cancer Cells to the Cold Atmospheric Plasma-Stimulated Solutions *Sci. Rep.* **7** 4479

[28] Tanaka H, Nakamura K, Mizuno M, Ishikawa K, Takeda K, Kajiyama H, Utsumi F, Kikkawa F and Hori M 2016 Non-thermal atmospheric pressure plasma activates lactate in Ringer's solution for anti-tumor effects *Sci. Rep.* **6** 36282

[29] Matsuzaki T, Kano A, Kamiya T, Hara H and Adachi T 2018 Enhanced ability of plasma-activated lactated Ringer's solution to induce A549 cell injury *Arch. Biochem. Biophys.* **656** 19–30

[30] Subramanian P S G, Jain A, Shivapuji A M, Sundaresan N R, Dasappa S and Rao L 2020 Plasma-activated water from a dielectric barrier discharge plasma source for the selective treatment of cancer cells *Plasma Process. Polym.* **17** 1900260

[31] Li Y, Kang M H, Uhm H S, Lee G J, Choi E H and Han I 2017 Effects of atmospheric-pressure non-thermal bio-compatible plasma and plasma activated nitric oxide water on cervical cancer cells *Sci. Rep.*

[32] Kumar N, Attri P, Dewilde S and Bogaerts A 2018 Inactivation of human pancreatic ductal adenocarcinoma with atmospheric plasma treated media and water: a comparative study *J. Phys. D. Appl. Phys.* **51** 255401

[33] Shimizu Y, Kinoshita I, Kikuchi J, Yamazaki K, Nishimura M, Birrer M J and Dosaka-Akita H 2008 Growth inhibition of non-small cell lung cancer cells by AP-1 blockade using a cJun dominant-negative mutant *Br. J. Cancer* **98** 915–22

[34] Attri P, Kim Y H, Park D H, Park J H, Hong Y J, Uhm H S, Kim K N, Fridman A and Choi E H 2015 Generation mechanism of hydroxyl radical species and its lifetime prediction during the plasma-initiated ultraviolet (UV) photolysis *Sci. Rep.* **5** 9332

[35] Attri P, Yusupov M, Park J H, Lingamdinne L P, Koduru J R, Shiratani M, Choi E H and Bogaerts A 2016 Mechanism and comparison of needle-type non-thermal direct and indirect atmospheric pressure plasma jets on the degradation of dyes *Sci. Rep.* **6** 34419

[36] Attri P, Han J, Choi S, Choi E H, Bogaerts A and Lee W 2018 CAP modifies the structure of a model protein from thermophilic bacteria: mechanisms of CAP-mediated inactivation *Sci. Rep.* **8** 10218

[37] Diehl K-H, Hull R, Morton D, Pfister R, Rabemampianina Y, Smith D, Vidal J-M and Vorstenbosch C Van De 2001 A good practice guide to the administration of substances and removal of blood, including routes and volumes *J. Appl. Toxicol.* **21** 15–23

[38] Workman P, Aboagye E O, Balkwill F, Balmain A, Bruder G, Chaplin D J, Double J A, Everitt J, Farningham D A H, Glennie M J, Kelland L R, Robinson V, Stratford I J, Tozer G M, Watson S, Wedge S R and Eccles S A 2010 Guidelines for the welfare and use of animals in cancer research *Br. J. Cancer* **102** 1555–77

[39] Flecknell P A 1996 *Laboratory animal anaesthesia : a practical introduction for research workers and technicians* (Academic Press)

[40] Dourish C T 1987 Effects of Drugs on Spontaneous Motor Activity *Experimental Psychopharmacology* (Totowa, NJ: Humana Press) pp 153–211

[41] Kim H-S, Park S-I, Choi S-H, Song C-H, Park S-J, Shin Y-K, Han C-H, Lee Y J and Ku S-K 2015 Single Oral Dose Toxicity Test of Blue Honeysuckle Concentrate in Mice *Toxicol. Res.* **31** 61–8

[42] Lee J-Y, Lee Y-M, Chang G-C, Yu S-L, Hsieh W-Y, Chen J J W, Chen H-W and Yang P-C 2011 Curcumin Induces EGFR Degradation in Lung Adenocarcinoma and Modulates p38 Activation in Intestine: The Versatile Adjuvant for Gefitinib Therapy ed M Blagosklonny *PLoS One* **6** e23756

[43] Nishimura G, Yanoma S, Mizuno H, Kawakami K and Tsukuda M 1999 An antioxidant, probucol, induces anti-angiogenesis and apoptosis in athymic nude mouse xenografted human head and neck squamous carcinoma cells *Japanese J. Cancer Res.* **90** 1224–30

[44] Zarling J M, Schlais J, Eskra L, Greene J J, Ts'o P O and Carter W A 1980 Augmentation of human natural killer cell activity by polyinosinic acid-polycytidylic acid and its nontoxic mismatched analogues *J. Immunol.* **124** 1852–7

[45] Strayer D R, Carter W A, Mayberry S D, Pequignot E and Brodsky I 1984 Low Natural Cytotoxicity of Peripheral Blood Mononuclear Cells in Individuals with High Familial Incidences of Cancer *Cancer Res.* **44** 370–4

[46] Hubbell H R, Kvalnes-Krick K, Carter W A and Strayer D R 1985 Antiproliferative and Immunomodulatory Actions of ^-Interferon and Double-Stranded RNA, Individually and in Combination, on Human Bladder Tumor Xenografts in Nude Mice *Cancer Res.*

[47] Yoon H S, Kim J W, Cho H R, Moon S B, Shin H D, Yang K J, Lee H S, Kwon Y S and Ku S K 2010 Immunomodulatory effects of Aureobasidium pullulans SM-2001 exopolymers on cyclophosphamide-treated mice *J. Microbiol. Biotechnol.* **20** 433–50

[48] Kim T H, Hur E G, Kang S J, Kim J A, Thapa D, Mie Lee Y, Ku S K, Jung Y and Kwak M K 2011 NRF2 blockade suppresses colon tumor angiogenesis by

inhibiting hypoxia-induced activation of HIF-1α *Cancer Res.* **71** 2260–75

[49] Park J C, Lee Y J, Choi H Y, Shin Y K, Kim J D and Ku S K 2014 In vivo and in vitro Antitumor effects of platycodin D, A saponin purified from platycodi radix on the H520 lung cancer cell *Evidence-based Complement. Altern. Med.* **2014** 1–17

[50] Choi J Y, Ramasamy T, Kim S Y, Kim J, Ku S K, Youn Y S, Kim J R, Jeong J H, Choi H G, Yong C S and Kim J O 2016 PEGylated lipid bilayer-supported mesoporous silica nanoparticle composite for synergistic co-delivery of axitinib and celastrol in multi-targeted cancer therapy *Acta Biomater.* **39** 94–105

[51] Zabłocka-Słowińska K, Porębska I, Gołecki M, Kosacka M, Pawełczyk K, Pawlik-Sobecka L, Zarębska K and Grajeta H 2016 Total antioxidant status in lung cancer is associated with levels of endogenous antioxidants and disease stage rather than lifestyle factors – preliminary study *Współczesna Onkol.* **4** 302–7

[52] Lee W H, Gam C O, Ku S K and Choi S H 2011 Single oral dose toxicity test of platycodin D, a saponin from platycodin radix in mice *Toxicol. Res.* **27** 217–24

[53] Song Y, Xiao Z, Wang K, Wang X, Zhang C, Fang F, Sun X and Shen B 2017 Development and Evaluation of 18F-IRS for Molecular Imaging Mutant EGF Receptors in NSCLC *Sci. Rep.* **7** 3121

[54] Cairns R A, Harris I S and Mak T W 2011 Regulation of cancer cell metabolism *Nat. Rev. Cancer* **11** 85–95

[55] Liou G-Y and Storz P 2010 Reactive oxygen species in cancer. *Free Radic. Res.* **44** 479–96

[56] Tucker M R and Watzke I M 1991 Autogenous auricular cartilage graft for temporomandibular joint repair: A comparison of technique with and without temporary silastic implantation *J. Cranio-Maxillofacial Surg.* **19** 108–12

[57] Wu J, Min R, Wu M and Chen W 2011 Gefitinib induces mitochondrial-dependent apoptosis in Saccharomyces cerevisiae *Mol. Med. Rep.* **4** 357–62

[58] Paulsen C E, Truong T H, Garcia F J, Homann A, Gupta V, Leonard S E and Carroll K S 2012 Peroxide-dependent sulfenylation of the EGFR catalytic site enhances kinase activity *Nat. Chem. Biol.* **8** 57–64

[59] Liu T-C, Jin X, Wang Y and Wang K 2017 Role of epidermal growth factor receptor in lung cancer and targeted therapies. *Am. J. Cancer Res.* **7** 187–202

[60] Leung E L-H, Fan X-X, Wong M P, Jiang Z-H, Liu Z-Q, Yao X-J, Lu L-L, Zhou Y-L, Yau L-F, Tin V P-C and Liu L 2016 Targeting Tyrosine Kinase Inhibitor-Resistant Non-Small Cell Lung Cancer by Inducing Epidermal Growth Factor Receptor Degradation *via* Methionine 790 Oxidation *Antioxid. Redox Signal.* **24** 263–79

[61] Lee H Y, Parkinson E I, Granchi C, Paterni I, Panigrahy D, Seth P, Minutolo F and Hergenrother P J 2017 Reactive Oxygen Species Synergize To Potently and

Selectively Induce Cancer Cell Death *ACS Chem. Biol.* **12** 1416–24

[62] Verfaillie T, Rubio N, Garg A D, Bultynck G, Rizzuto R, Decuypere J-P, Piette J, Linehan C, Gupta S, Samali A and Agostinis P 2012 PERK is required at the ER-mitochondrial contact sites to convey apoptosis after ROS-based ER stress *Cell Death Differ.* **19** 1880–91

[63] Liang S-H, Zhang W, Mcgrath B C, Zhang P and Cavener D R 2006 PERK (eIF2α kinase) is required to activate the stress-activated MAPKs and induce the expression of immediate-early genes upon disruption of ER calcium homoeostasis *Biochem. J.* **393** 201–9

[64] Fearon K C H, Glass D J and Guttridge D C 2012 Cancer cachexia: Mediators, signaling, and metabolic pathways *Cell Metab.* **16** 153–66

[65] Chang C H, Qiu J, O'Sullivan D, Buck M D, Noguchi T, Curtis J D, Chen Q, Gindin M, Gubin M M, Van Der Windt G J W, Tonc E, Schreiber R D, Pearce E J and Pearce E L 2015 Metabolic Competition in the Tumor Microenvironment Is a Driver of Cancer Progression *Cell* **162** 1229–41

[66] Clark J C M, Dass C R and Choong P F M 2009 Development of chondrosarcoma animal models for assessment of adjuvant therapy *ANZ J. Surg.* **79** 327–36

[67] Kennedy J D, Pierce C W and Lake J P 1992 Extrathymic T cell maturation. Phenotypic analysis of T cell subsets in nude mice as a function of age. *J. Immunol.* **148** 1620–9

[68] Fearon K C H, Mcmillan D C, Preston T, Winstanley F P, Cruickshank A M and Shenkin A 1991 Elevated circulating interleukin-6 Is associated with an acute-phase response but reduced fixed hepatic protein synthesis in patients with cancer *Ann. Surg.* **213** 26–31

[69] Chang C-H, Lee C-H, Ko J-C, Chang L-Y, Lee M-C, Wang J-Y and Yu C-J 2017 Gefitinib or erlotinib in previously treated non-small-cell lung cancer patients: a cohort study in Taiwan *Cancer Med.* **6** 1563–72

[70] Weng M-S, Chang J-H, Hung W-Y, Yang Y-C and Chien M-H 2018 The interplay of reactive oxygen species and the epidermal growth factor receptor in tumor progression and drug resistance *J. Exp. Clin. Cancer Res.* **37** 61

[71] Mateu-Sanz M, Tornín J, Brulin B, Khlyustova A, Ginebra M P, Layrolle P and Canal C 2020 Cold plasma-treated ringer's saline: A weapon to target osteosarcoma *Cancers (Basel).*

[72] Xu D, Wang B, Xu Y, Chen Z, Cui Q, Yang Y, Chen H and Kong M G 2016 Intracellular ROS mediates gas plasma-facilitated cellular transfection in 2D and 3D cultures *Sci. Rep.* **6** 27872

[73] Turrini E, Laurita R, Stancampiano A, Catanzaro E, Calcabrini C, Maffei F, Gherardi M, Colombo V and Fimognari C 2017 Cold Atmospheric Plasma Induces Apoptosis and Oxidative Stress Pathway Regulation in T-

Lymphoblastoid Leukemia Cells *Oxid. Med. Cell. Longev.* **2017** 1–13

[74] Kumar N, Shaw P, Uhm H S, Choi E H and Attri P 2017 Influence of Nitric Oxide generated through microwave plasma on L6 skeletal muscle cell myogenesis via oxidative signaling pathways *Sci. Rep.* **7** 542

[75] Bekeschus S, Lippert M, Diepold K, Chiosis G, Seufferlein T and Azoitei N 2019 Physical plasma-triggered ROS induces tumor cell death upon cleavage of HSP90 chaperone *Sci. Rep.*

[76] Moniruzzaman R, Rehman M U, Zhao Q-L, Jawaid P, Mitsuhashi Y, Imaue S, Fujiwara K, Ogawa R, Tomihara K, Saitoh J, Noguchi K, Kondo T and Noguchi M 2018 Roles of intracellular and extracellular ROS formation in apoptosis induced by cold atmospheric helium plasma and X-irradiation in the presence of sulfasalazine *Free Radic. Biol. Med.* **129** 537–47

[77] Bauer G 2015 Increasing the endogenous NO level causes catalase inactivation and reactivation of intercellular apoptosis signaling specifically in tumor cells *Redox Biol.* **6** 353–71

[78] Bauer G 2018 Targeting Protective Catalase of Tumor Cells with Cold Atmospheric Plasma- Activated Medium (PAM) *Anticancer. Agents Med. Chem.* **18** 784–804

[79] Zhuang S, Demirs J T and Kochevar I E 2001 Protein kinase C inhibits singlet oxygen-induced apoptosis by decreasing caspase-8 activation *Oncogene* **20** 6764–76

[80] Escobar J A, Rubio M A and Lissi E A 1996 SOD and catalase inactivation by singlet oxygen and peroxyl radicals *Free Radic. Biol. Med.* **20** 285–90

[81] Kim S Y, Kwon O J and Park J W 2001 Inactivation of catalase and superoxide dismutase by singlet oxygen derived from photoactivated dye. *Biochimie* **83** 437–44

[82] Backman L J and Danielson P 2013 Akt-mediated anti-apoptotic effects of substance P in Anti-Fas-induced apoptosis of human tenocytes *J. Cell. Mol. Med.* **17** 723–33

[83] Satooka H and Hara-Chikuma M 2016 Aquaporin-3 Controls Breast Cancer Cell Migration by Regulating Hydrogen Peroxide Transport and Its Downstream Cell Signaling *Mol. Cell. Biol.* **36** 1206–18

[84] Scheit K and Bauer G 2014 Direct and indirect inactivation of tumor cell protective catalase by salicylic acid and anthocyanidins reactivates intercellular ROS signaling and allows for synergistic effects *Carcinogenesis* **36** 400–11

Figure Captions

Figure 1. Schematic diagram of the atmospheric pressure plasma jet. Atmospheric pressure plasma jet was used here (A), current-voltage graph indicated in (B), OES spectrum (C) and RONS data (D).

Figure 2. Schematic illustration of PTW uses *in vitro* and *in vivo* studies (A) and experimental procedure of anticancer *in vivo* studies (B).

Figure 3. Antitumor effect of PTW and gefitinib. NCI-H520 cells were treated with plasma-treated water (PTW, A) or with gefitinib (B) at the indicated doses for 72 hrs. The cell viability was compared with that of non-treatment and expressed as the mean ± S.D. (six independent assays). The probable mechanism of anticancer effect of PTW shown in (C)

Figure 4. Body weight changes and tumor growth. NCI-H520 xenograft tumor bearing (TB) mice were orally administered with distilled water (TB control), gefitinib or PTW at 2.0, 1.0 and 0.5 ml/kg (PTW2.0, PTW1.0 and PTW0.5, respectively). Kinetic changes of body weight (A) and tumor volume (vol.) (B) were assessed, and the tumor was exposed after treatment for 35 days (C). Scale bars indicate 15 mm. Body weight excluding the tumor was assessed, and weight gains were calculated by subtracting body weights at pre-treatment from day 35 post-treatment (D). Then, the absolute tumor weight (E) and the relatives to the body weights (F) were assessed. The values are expressed as the mean ± S.D. (eight mice per group). ‡ $p<0.01$ versus intact group, and ** $p<0.01$ and * $p<0.05$ versus the TB control group. The kinetic analyses were examined by two-way ANOVA, and others were by one-way ANOVA, followed by LSD post hoc tests.

Figure 5. Effects on immune responses. Levels of serum (A) and splenic (B) cytokines were assessed. The cytokines include interleukin (IL)-6, interferon (IFN), tumor necrosis factor (TNF)-α, IL-1 and IL-10. The activity of splenic and peritoneal natural killer (NK) cell was assessed by a chromium (^{51}Cr) release assay. The values are expressed as the mean ± S.D. (eight mice samples per group). ‡ $p<0.01$ and †

$p<0.05$ versus intact group, and ** $p<0.01$ versus the TB control group, by non-parametric analyses followed by the Mann-Whitney U post-hoc test for data of IL-6 and IFN-γ or by one-way ANOVA followed by LSD post hoc tests for others.

Figure 6. Effects on tumor mass. Tumor tissue was stained with hematoxylin and eosin, and the representative pictures are shown as low- and high-magnification on the left and right, respectively (A). Dotted area indicates necrotic tissues in the tumor mass. Scale bars indicate 100 μm. The tumor cell area was assessed, and the values are expressed as the mean ± S.D. (eight mice samples per group) (B). ** $p<0.01$ versus the TB control group, by one-way ANOVA followed by LSD post hoc tests.

Figure 7. Immunohistochemistry in tumor mass. Tumor tissue was immunostained for caspase-3 and poly (ADP-ribose) polymerase (PARP) (for apoptosis), Ki-67 and cluster of differentiation (CD)31 (for cell proliferation and angiogenesis, respectively), nitrotyrosine (NT) and 4-hydroxynonenal (4HNE) (for oxidative stress), and inducible nitric oxide synthases (iNOS) and tumor necrosis factor (TNF)-α (for immune activities) (A). Scale bars indicate 100 μm. The percentage of immune-reactive cells are shown in (B-E). The values are expressed as the mean ± S.D. (eight mice samples per group). ** $p<0.01$ versus the TB control group, by one-way ANOVA followed by LSD post hoc tests.

Figure 8. Effects on the immune organs and fat tissues. Representative pictures for immune organs of spleen and lymph node and fat tissue are shown in low- and high-magnification on the left and right, respectively. Arrows indicate lymphoid follicles in the spleen and lymph node, and dotted line is for a range of the fat tissue. Scale bars indicate 400 μm in the spleen and lymph node, and 100 μm in the fat tissues. WP = white pulp, RP = red pulp, G = secondary follicle, CO = cortex, ME = medullar, FO = follicle.

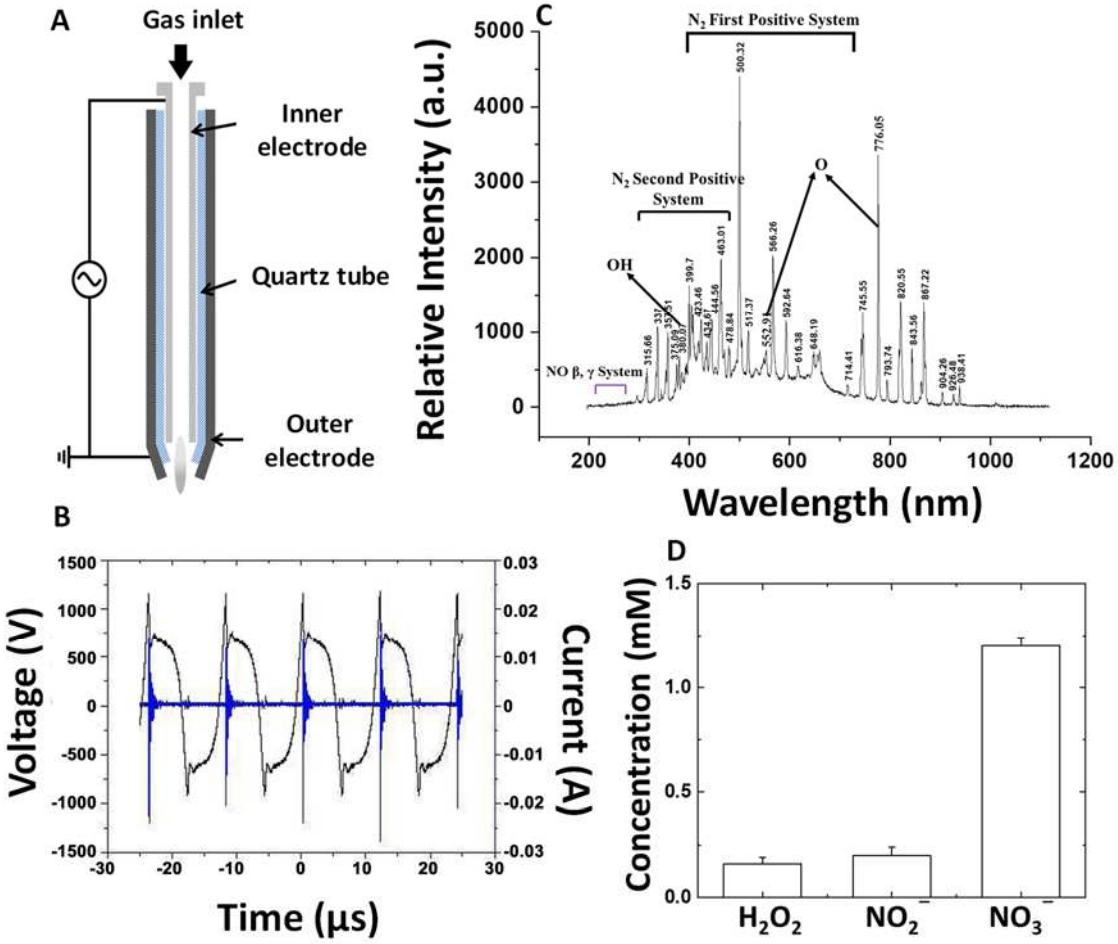
A
Gas inlet
Inner electrode
Quartz tube
Outer electrode
B
Voltage (V)
Current (A)
Time (μs)
C
Relative Intensity (a.u.)
Wavelength (nm)
N2 First Positive System
N2 Second Positive System
OH
O
NO β, γ System
D
Concentration (mM)
H2O2
NO2−
NO3−

Figure 1.

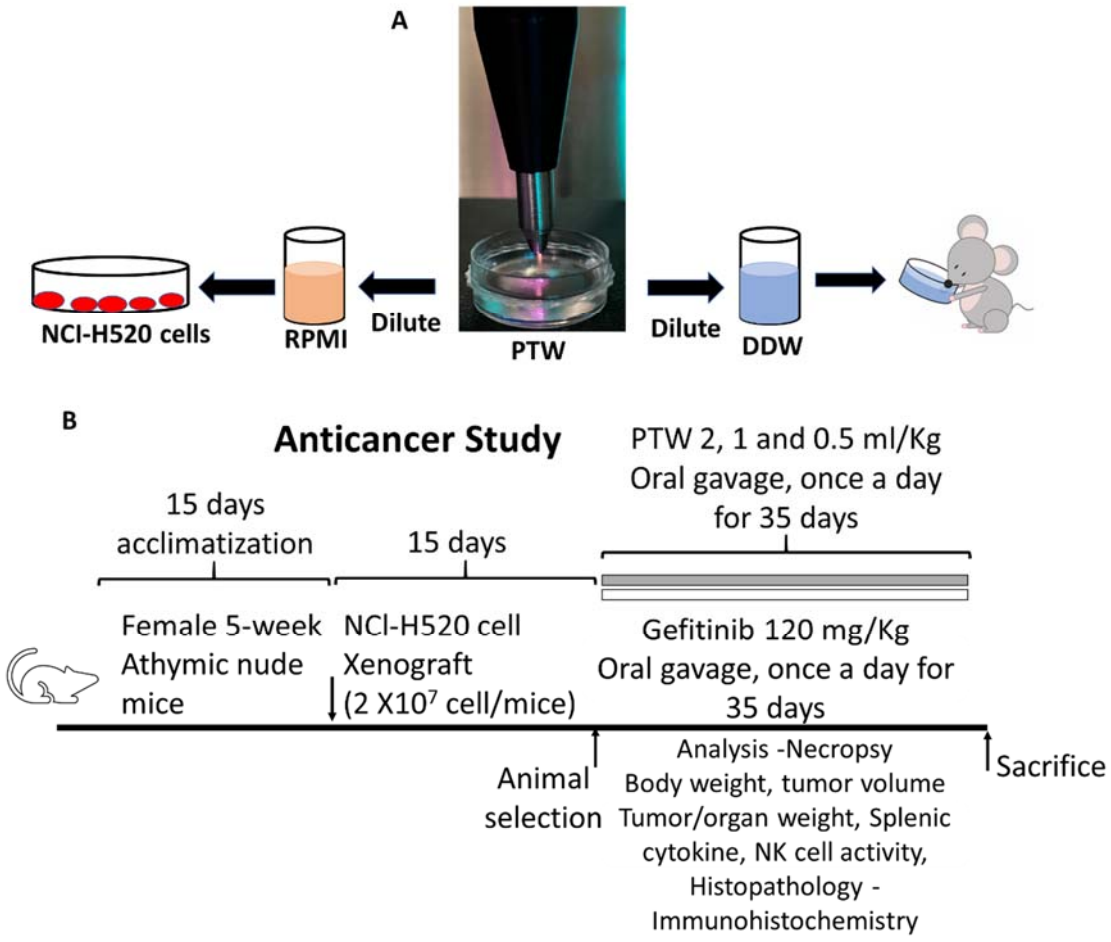
A
NCI-H520 cells
RPMI
Dilute
PTW
Dilute
DDW
B
Anticancer Study
PTW 2, 1 and 0.5 ml/Kg
Oral gavage, once a day
for 35 days
15 days
acclimatization
15 days
Female 5-week
Athymic nude
mice
NCI-H520 cell
Xenograft
(2 X10⁷ cell/mice)
Gefitinib 120 mg/Kg
Oral gavage, once a day for
35 days
Animal
selection
Analysis -Necropsy
Body weight, tumor volume
Tumor/organ weight, Splenic
cytokine, NK cell activity,
Histopathology -
Immunohistochemistry
Sacrifice

Figure 2

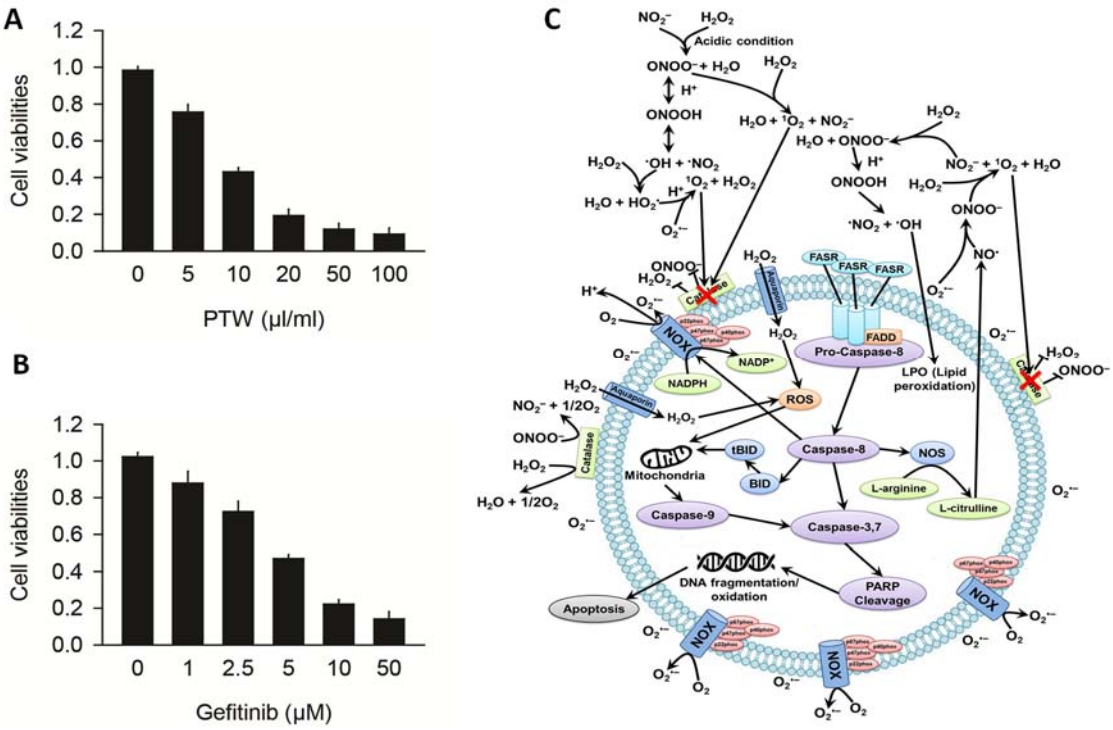
A
Cell viabilities
1.2
1.0
0.8
0.6
0.4
0.2
0.0
0
5
10
20
50
100
PTW (μl/ml)
B
Cell viabilities
1.2
1.0
0.8
0.6
0.4
0.2
0.0
0
1
2.5
5
10
50
Gefitinib (μM)
C
Acidic condition
ONOOH
FASR
FADD
Pro-Caspase-8
LPO (Lipid peroxidation)
NADPH
NADP+
ROS
Aquaporin
Catalase
Mitochondria
tBID
BID
Caspase-8
NOS
L-arginine
L-citrulline
Caspase-9
Caspase-3,7
DNA fragmentation/ oxidation
PARP Cleavage
Apoptosis
NOX

Figure 3.

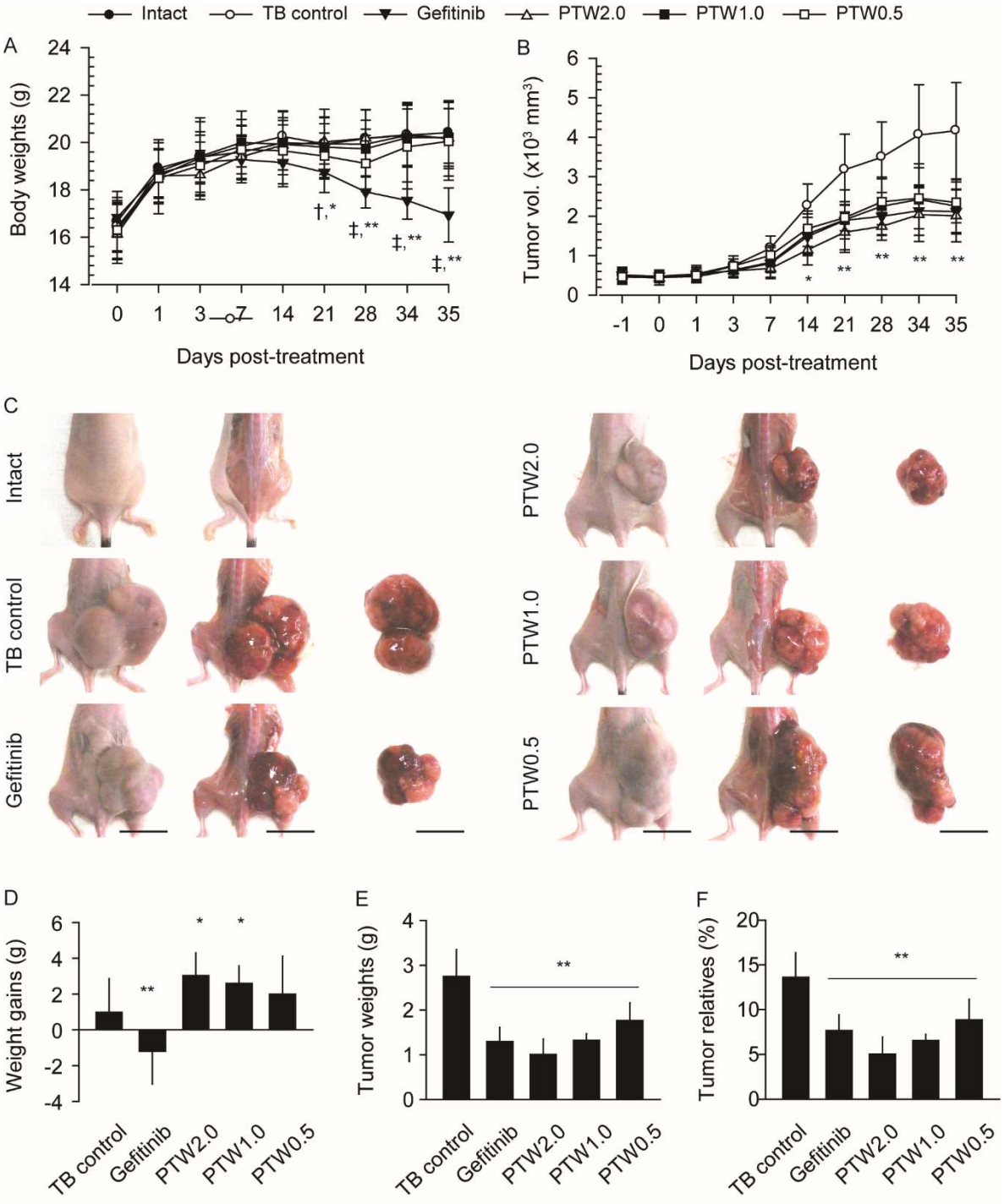
Intact
TB control
Gefitinib
PTW2.0
PTW1.0
PTW0.5
A
Body weights (g)
Days post-treatment
B
Tumor vol. (x10³ mm³)
Days post-treatment
C
Intact
TB control
Gefitinib
PTW2.0
PTW1.0
PTW0.5
D
Weight gains (g)
E
Tumor weights (g)
F
Tumor relatives (%)
TB control
Gefitinib
PTW2.0
PTW1.0
PTW0.5

Figure 4.

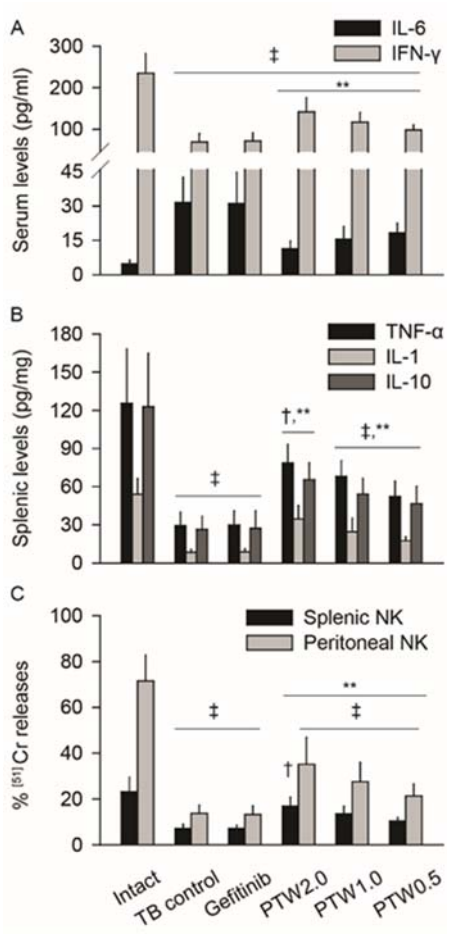
A
IL-6
IFN-γ
Serum levels (pg/ml)
300
200
100
45
30
15
0
‡
**
B
TNF-α
IL-1
IL-10
Splenic levels (pg/mg)
180
150
120
90
60
30
0
†,**
‡,**
‡
C
Splenic NK
Peritoneal NK
% [51]Cr releases
100
80
60
40
20
0
**
‡
‡
†
Intact
TB control
Gefitinib
PTW2.0
PTW1.0
PTW0.5

Figure 5.

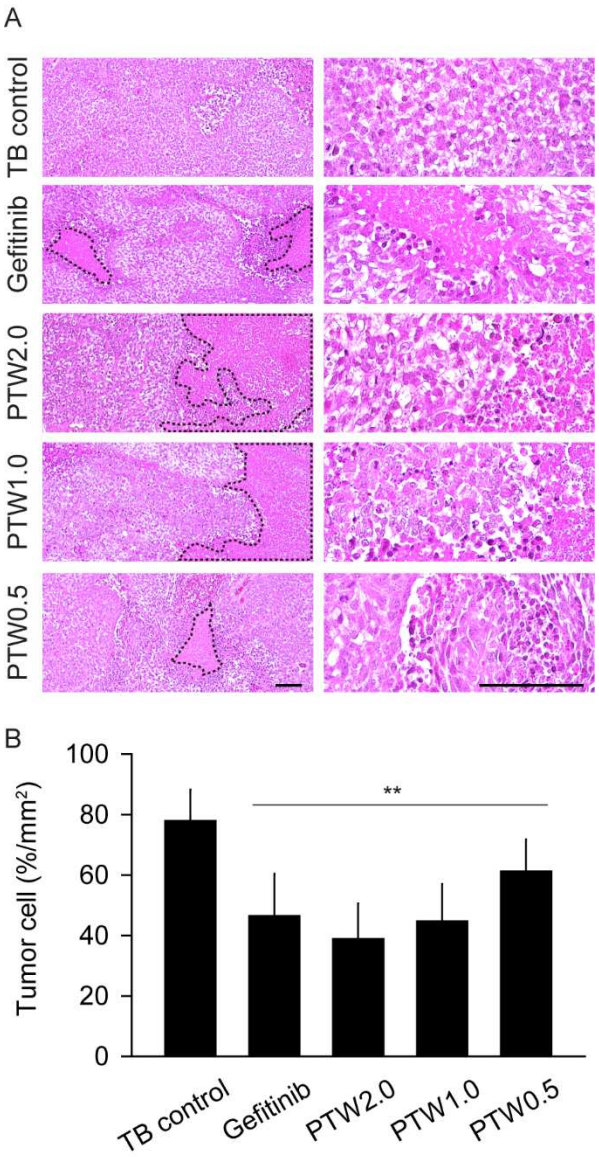
A
TB control
Gefitinib
PTW2.0
PTW1.0
PTW0.5
B
Tumor cell (%/mm²)
100
80
60
40
20
0
**
TB control
Gefitinib
PTW2.0
PTW1.0
PTW0.5

Figure 6.

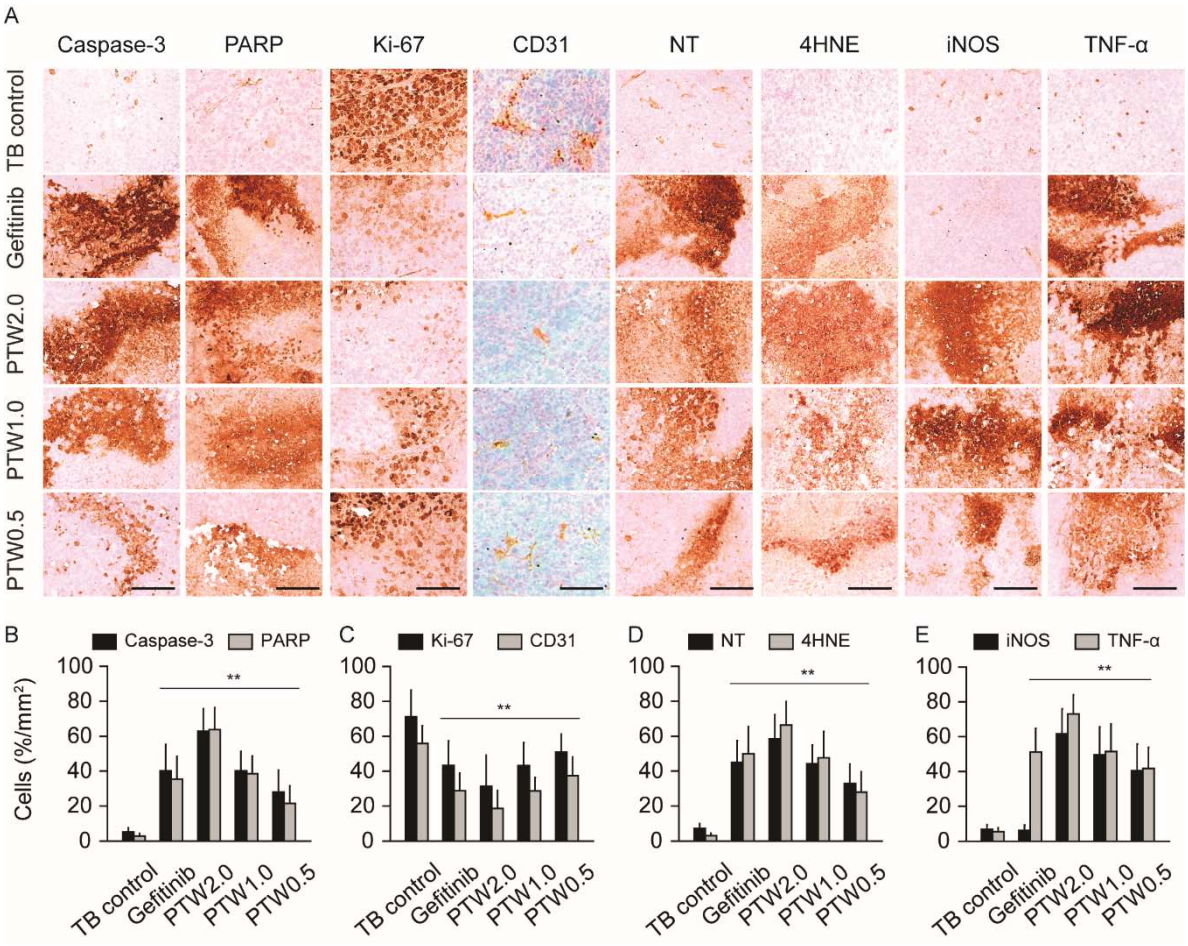
A
Caspase-3
PARP
Ki-67
CD31
NT
4HNE
iNOS
TNF-α
TB control
Gefitinib
PTW2.0
PTW1.0
PTW0.5
B
Caspase-3
PARP
Cells (%/mm²)
C
Ki-67
CD31
D
NT
4HNE
E
iNOS
TNF-α
**
TB control
Gefitinib
PTW2.0
PTW1.0
PTW0.5

Figure 7.

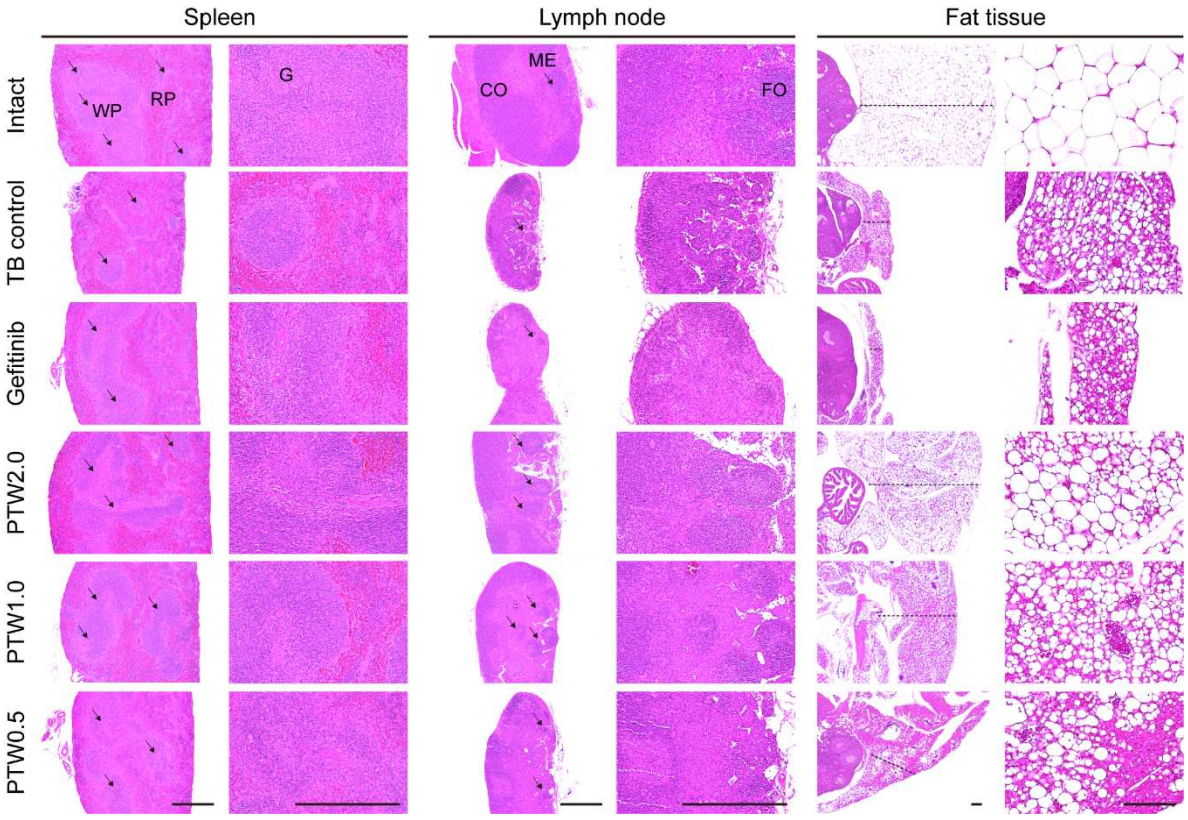
Spleen
Lymph node
Fat tissue
Intact
TB control
Gefitinib
PTW2.0
PTW1.0
PTW0.5
WP
RP
G
ME
CO
FO

Figure 8.

Table 1. Histopathological changes on the spleen, lymph node and periovarian fat tissues of NSCLC mice model.

	Intact	TB control	Gefitinib	PTW2.0	PTW1.0	PTW0.5
Spleen						
Thickness (mm)	1.70±0.15	1.07±0.11‡	1.13±0.16‡	1.54±0.13†,**	1.36±0.10‡,**	1.26±0.13‡,**
White pulps (n/mm^2)	14.88±2.23	5.63±1.69‡	5.75±1.28‡	11.75±2.25‡,**	10.00±1.15‡,**	8.88±1.25‡,**
White pulp diameters (μm)	693.67±119.95	289.92±43.78‡	296.18±30.08‡	531.81±72.25‡,**	454.87±78.85‡,**	361.05±40.85‡,**
Lymph node						
Thickness (mm)	0.99±0.16	0.44±0.13‡	0.46±0.14‡	0.81±0.14‡,**	0.75±0.10‡,**	0.64±0.76‡,**
Lymph follicles (n/mm^2)	23.50±5.26	6.38±1.51‡	6.88±1.46‡	16.50±2.33‡,**	14.88±3.14‡,**	12.75±3.88‡,**
Cortex thickness (μm)	508.49±91.98	163.24±52.84‡	150.62±77.30‡	340.43±77.56‡,**	275.93±65.54‡,**	238.55±44.96‡,*
Fat tissues						
Thickness (mm)	1.82±0.35	0.27±0.11‡	0.25±0.11‡	1.19±0.22‡,**	0.67±0.11‡,**	0.59±0.13‡,**
Adipocyte diameters (μm)	67.68±15.83	12.64±3.35‡	13.66±3.58‡	35.67±7.41‡,**	23.90±4.70‡,**	18.10±3.01‡,**

The values are expressed as the mean ± S.D. for eight mice. ‡ $p<0.01$ and † $p<0.05$ versus the intact group and ** $p<0.01$ and * $p<0.05$ versus the TB control group, by one-way ANOVA followed by LSD post hoc tests.